Ability of a low-dimensional model to predict geometry-dependent dynamics of large-scale coherent structures in turbulence

Kunlun Bai, Dandan Ji, and Eric Brown

A low-dimensional model can predict geometry-dependent dynamics of large-scale coherent structures in turbulence

Kunlun Bai, Dandan Ji, and Eric Brown

Department of Mechanical Engineering and Materials Science, Yale University, New Haven, CT 06511, USA

We test the ability of a general low-dimensional model for turbulence to predict geometry-dependent dynamics of large-scale coherent structures, such as convection rolls. The model consists of stochastic ordinary differential equations, which are derived as a function of boundary geometry from the Navier-Stokes equations [1, 2]. We test the model using Rayleigh-Bénard convection experiments in a cubic container. The model predicts a mode in which the alignment of a convection roll stochastically crosses a potential barrier to switch between diagonals. We observe this mode with a measured switching rate within 30% of the prediction.

Large-scale coherent flow structures in turbulence – such as convection rolls in the atmosphere – are ubiquitous and can play a dominant role in heat and mass transport. A particular challenge is to predict dynamical states and their change with different boundary geometries, for example in the way that convection rolls in the atmosphere can be affected by topography such as mountain ranges [3]. However, the Navier-Stokes equations that describe flows are impractically difficult to solve for turbulent flows, so low-dimensional models are desired.

It has long been recognized that the dynamical states of large-scale coherent structures are similar to those of low-dimensional dynamical systems models [4] and stochastic ordinary differential equations [5–8]. However, such models tend to be descriptive rather than predictive, as parameters are typically fitted to observations, rather than derived [9]. In particular, dynamical systems models tend to fail at quantitative predictions of new dynamical states in regimes outside where they were parameterized. In this paper we demonstrate a proof-of-principle that a general low dimensional model can quantitatively predict the different dynamical states of large-scale coherent structures in different geometries.

The model system is Rayleigh-Bénard convection, in which a fluid is heated from below and cooled from above to generate buoyancy-driven convection [10, 11]. This system exhibits robust large-scale coherent structures that retain the same organized flow structure over long times. For example, in upright cylindrical containers of aspect ratio 1, a large-scale circulation (LSC) forms. This LSC consists of temperature and velocity fluctuations which, when coarse-grain averaged, collectively form a single convection roll in a vertical plane [12], as shown in Fig. 1a. Various dynamics of the LSC have been reported, including spontaneous meandering of the orientation θ_0 in a horizontal plane, and an advected oscillation which appears as a torsional or sloshing mode [13–19]. As an example of different dynamical states in different geometries, if instead the axis of the cylinder is aligned horizontally, θ_0 tends to align with the longest diagonals of the cell, and oscillates periodically between diagonals and around individual corners [20].

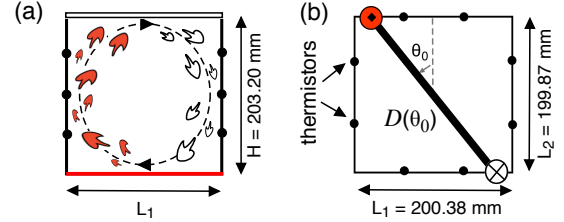While there are several low-dimensional models for LSC dynamics [21–24], only one by Brown & Ahlers

FIG. 1. (a) A side view of the large-scale circulation (LSC), indicated by the dashed line. Hot and cold features are filled with red (online) and white, respectively. (b) Top view of a horizontal cross-section at mid-height of the cubic container. Thermistor locations on the side wall are indicated by small circles. The orientation of the LSC is defined as the angle θ_0 between the hot side of the circulation plane (thick solid line) and the vertical dashed line. The length of the circulation plane across a horizontal cross-section $D(\theta_0)$ determines the model potential.

has made predictions dependent on container geometry [1, 2, 5]. The model consists of a pair of stochastic ordinary differential equations, using the empirically known, robust LSC structure as an approximate solution to the Navier-Stokes equations. The resulting dynamical equation for θ_0 is

$$\ddot{\theta}_0 = -\frac{\dot{\theta}_0 \delta}{\tau_{\dot{\theta}} \delta_0} - \nabla V_g(\theta_0) + f_{\dot{\theta}}(t) \ . \tag{1}$$

The first term on the right is a damping term where $\tau_{\dot{\theta}}$ is a damping time scale. A separate stochastic ordinary differential equation describes the fluctuations of δ around its stable fixed point δ_0 [1]. $f_{\dot{\theta}}$ is a stochastic forcing term representing the effect of small-scale turbulent fluctuations and is modeled as Gaussian white noise with diffusivity $D_{\dot{\theta}}$. This model is mathematically equivalent to diffusion in a potential landscape $V_g(\theta_0)$. The potential V_g represents the pressure of the sidewalls acting on the LSC, and is given by

$$V_g(\theta_0) = \left\langle \frac{3\omega_\phi^2 H^2}{4D(\theta_0)^2} \right\rangle_\gamma \tag{2}$$
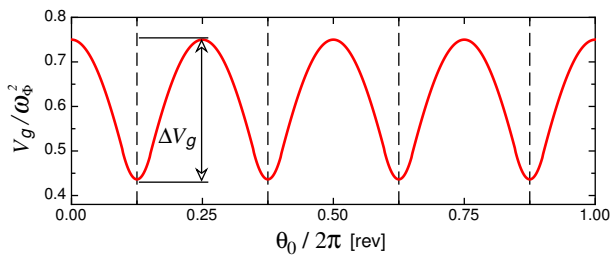
FIG. 2. The model potential $V_g(\theta_0)$ for a cubic cell (Eq. 2). The vertical dashed lines indicate the location of the four corners where the potential minima occur. Eq. 1 describes diffusive fluctuations of θ_0 in this potential, which can occasionally cross the barriers ΔV_g to switch between corners.

FIG. 3. Normalized temperature profiles when $\theta_0 = 1/8$ $rev.$ (circles filled with red, online); and $\theta_0 = 1/4$ $rev.$ (open diamonds). Line: cosine fitting function from which the normalization parameters are obtained. The fits are equally good, indicating the structure of the LSC is similar at both the potential minimum ($\theta_0 = 1/8$ $rev.$) and potential maximum ($\theta_0 = 1/4$ $rev.$).

where ω_ϕ is the turnover frequency of the LSC, and H is the height of the container [2]. This includes an update to [2] of the numerical coefficient for aspect ratio 1 containers [20]. The notation $\langle ... \rangle_\gamma$ represents a uniformly weighted smoothing of the potential over the width $\gamma = \pi/10$ of the LSC [20]. $D(\theta_0)$ is the distance across a horizontal cross-section of the cell, as a function of θ_0, illustrated in Fig. 1b. Thus, $D(\theta_0)$, and consequently V_g and Eq. 1 can be predicted explicitly for any system geometry, with the caveat that in this form of the model the geometry must support a single-roll LSC.

This model and its extensions have successfully described all of the known dynamics of the LSC [1, 2, 5, 18, 20, 25, 26]. Since the model is derived from the Navier-Stokes equations, the model terms can be predicted and are typically accurate within a factor of 2. The only required fit parameter is $D_{\dot\theta}$ which can be fitted to independent measurements [1]. The model has described dynamics dependent on the geometric potential V_g [20], although in that case a correction was made to V_g for the nonzero width of the LSC, and another parameter was fitted to better describe data. Since the model was adjusted to describe results after they were observed, it has not yet been shown that the model can predict geometry-dependent dynamics before their observation.

In this paper, we test the model prediction of a switching of θ_0 between potential wells corresponding to a stochastic crossing of a potential barrier in θ_0 [2]. While it has been mentioned that a switching between corners has been observed [27], no data has been published before, and thus no models have been tested. There are also several possible different types of orientation switching that have been proposed in the literature, including reversals [23], cessations [5], periodic oscillations between corners [20], and stochastic crossing of a potential barrier in θ_0 [1], and it remains to be determined which occur in a cubic cell. We test the model prediction of stochastic switching in a cubic container which has 4 potential wells and 4 potential barriers ΔV_g of equal height, shown in Fig. 2 as calculated from Eq. 2. The cubic geometry prevents a competing periodic oscillation mode, which could occur if one potential barrier is smaller such that the
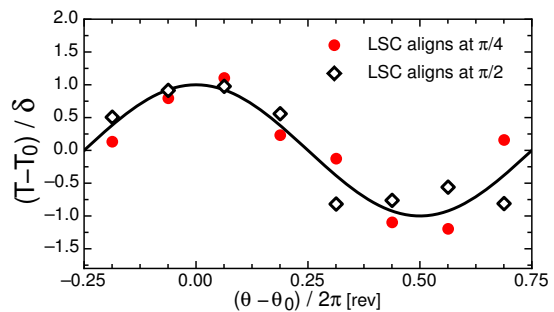
system could oscillate in the wider well surrounding two corners [20]. This is the first example of testing a quantitative prediction of a geometry-dependent mode of the LSC (i.e. the existence and properties of a mode that did not exist in other geometries studied) without any flexibility or free parameters in the geometry-dependence of the model.

I. METHODS

The cubic container is based on the design of [28]. It has dimensions $H = 203.20$ mm, $L_1 = 200.38$ mm, and $L_2 = 199.87$ mm, illustrated in Fig. 1. The variation of the cell dimensions due to bowing of the sidewall, epoxy to seal gaps and cover thermistors, and holes for filling water are each less than 0.7 mm. The cell is filled with degassed and deionized water at mean temperature 23.0 ^oC, for a Prandtl number $Pr \equiv \nu/\kappa = 6.4$ (κ is the thermal diffusivity, and ν is the kinematic viscosity). We report measurements at Rayleigh number $Ra \equiv \alpha g \Delta T H^3 / \kappa \nu = 4.8 \times 10^8$ ($\Delta T = 3.8$ ^oC is the temperature difference between top and bottom plate, α is the isobaric thermal expansion coefficient, and g is the acceleration of gravity). The standard deviation of the plate temperature over space and time is $0.005\Delta T$. The cell is isolated from room temperature variations as in [28]. The cell level is adjusted so that the probability distributions of θ_0 has 4 peaks at the 4 corners with magnitudes within 50% of each other. We achieved this for a cell within 0.03 degrees of level.

Fluid temperature is recorded by thermistors placed in blind holes in the acrylic sidewall, within 0.5 mm of the fluid surface [14]. Three rows of thermistors are located at heights $H/4$, $H/2$, and $3H/4$ above the bottom plate as shown in Fig. 1a. They are equally spaced in angle θ as shown in Fig. 1b, such that the four corners are located at $\theta = \frac{1}{8}$, $\frac{3}{8}$, $\frac{5}{8}$, and $\frac{7}{8}$ rev. The relative error on thermis-
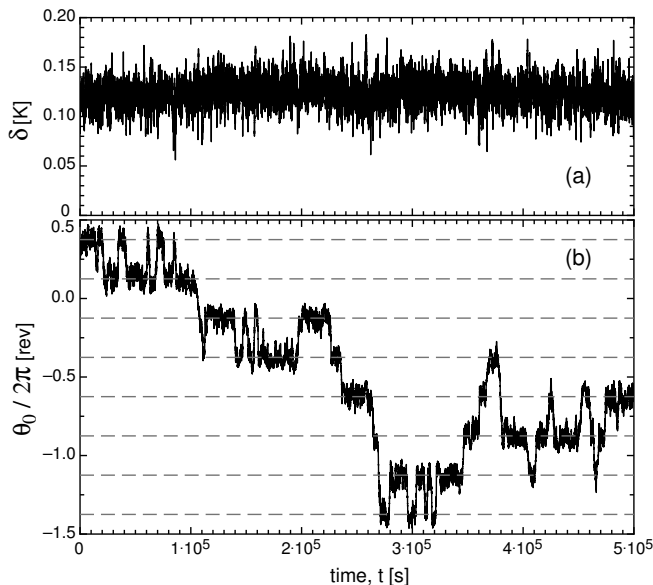
FIG. 4. Typical time series of the strength δ and the orientation θ_0 of the LSC in (a) and (b), respectively. The horizontal dashed lines in (b) indicate the locations of the four corners in the cubic container. Stochastic switching of θ_0 between corners is observed, as predicted [1].

tor measurements is 2.5 mK, which comes from a combination of the standard deviation of recorded temperature difference between thermistors during calibration (0.7 mK), temperature non-uniformity in the cell during calibration (1.2 mK), interpolation errors from fitting calibration temperatures (0.6 mK), drift of the thermistors between calibration runs (1.6 mK), and room temperature variations during experiments (1.2 mK). The LSC can be detected by the hot fluid it pulls up on one side and the cold fluid it pulls down the other side, as shown in Fig. 1a. The thermistor temperatures T are fitted by $T = T_0 + \delta cos(\theta - \theta_0)$ to obtain the LSC orientation θ_0, and half the horizontal temperature difference δ which characterizes the strength of the LSC, as in [14]. Examples of this fit are shown in Fig. 3

II. RESULTS

A typical time series of the strength δ and orientation θ_0 of the LSC at mid-plane ($H/2$) is shown in Fig. 4. Since θ_0 from all three planes track each other, they are always in the same potential well at the same time, which is all that is needed to identify switching, so we only present results from the mid-plane. θ_0 meanders erratically as in cylindrical containers [14, 15, 20]. θ_0 also prefers to align with the corners (dashed lines in Fig. 4b), which is different from upright cylindrical containers, and similar to previous measurements in rectangular containers [27, 29–33] and horizontal cylinders [20]. Such preference is expected since corners correspond to potential

minima (Fig. 2).

We also observe that θ_0 switches between corners, apparently randomly. The LSC samples all four corners in an irregular pattern, not just oscillating back and forth between two corners as observed by Song et al. [20]. We also observe that θ_0 does not tend to change by $1/2$ rev. during events, which would correspond to reversals; rather there is a strong preference for a change by $\pm 1/4$ rev. with each event. In previous studies it was found that θ_0 could reorient quickly due to cessation and reformation of the LSC, which is characterized by a drop of the LSC strength δ to effectively zero [34]. In the present study, δ fluctuates around its stable fixed point value $\delta_0 = 0.124\ K$ without dropping below $0.46\delta_0$, which indicates the switching observed here occurs without cessation. Fig. 3 shows a comparison of temperature profiles for $\theta_0 = 1/8\ rev$ and $\theta_0 = 1/4\ rev$., which correspond to a minimum and maximum of the potential, respectively. The fits are equally good in both cases. Averaged over the entire time series, the standard deviation between the measured temperature and the fit is 37 mK for the range $\theta_0 = 1/8 \pm 1/40\ rev$. (near a potential minimum) and 41 mK for the range $\theta = 1/4 \pm 1/40\ rev$. (near a potential maximum). This indicates that the LSC structure does not change much during the switching events. These qualitative observations are all consistent with the model prediction of stochastic switching across potential barriers, and inconsistent with the other proposed switching mechanisms [5, 20, 23].

To characterize the randomness of the switching, we measure the distribution of the time intervals τ_1 between switching events. When counting switching events we want to avoid counting extraneous events due to the jitter of θ_0 around a potential maximum or minimum. Thus, an event is not counted as soon as θ_0 crosses a potential maximum. Rather, for an event to be counted, θ_0 must not only cross a potential maximum, but also cross the orientation of the potential minimum of a well adjacent to the previous well an event was counted at. The probability distribution $P(\tau_1/\langle\tau_1\rangle)$ is shown in Fig. 5, where $\langle\tau_1\rangle$ is the average time interval between switching. The fractional error on each point is equal to the inverse square root of the number of events in each bin. Notably, there is no peak for $\tau_1 > 0$, confirming that the switching is not periodic as observed in Song et al. [20]. The data are consistent with the exponential function $P(\tau_1/\langle\tau_1\rangle) = exp(-\tau_1/\langle\tau_1\rangle)$ shown as the line in Fig. 5, which represents Poisson statistics, i.e. randomly distributed events in time, as predicted for the model of overdamped diffusion across a potential barrier [2].

For a quantitative prediction, the rate of switching between corners can be modeled as a fluctuation-driven crossing of a potential barrier. This was done previously [1] by simplifying Eq. 1 to the one solved by Kramers [35] by approximating $\delta = \delta_0$, which is valid if the fluctuations of δ around its stable fixed point δ_0 are small. In the overdamped limit, the number of switching events per unit time is given by
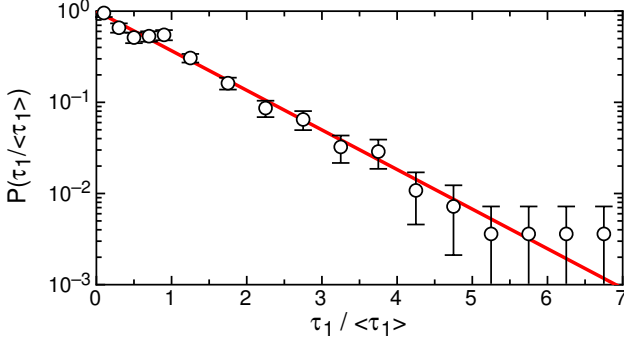
FIG. 5. The probability distribution $P(\tau_1/\langle\tau_1\rangle)$ of the time intervals between switching of θ_0 from one corner to another. Solid line: the function $P(\tau_1/\langle\tau_1\rangle) = \exp(-\tau_1/\langle\tau_1\rangle)$ representing a Poisson (random) distribution.

$$\omega = \frac{\sqrt{c_{min}c_{max}}\tau_{\dot\theta}}{2\pi}exp\left(-\frac{\Delta V_g}{D_{\dot\theta}\tau_{\dot\theta}}\right). \qquad (3)$$

$c_{min} = 15\omega_\phi^2/\pi$ and $c_{max} = 3\omega_\phi^2/2$ are the curvatures $|d^2V_g/d\theta^2|$ at the minimum and maximum of the potential, respectively. The potential barrier $\Delta V_g = \frac{3}{8}(1-\frac{\gamma}{2})\omega_\phi^2$ is calculated from Eq. 2 [20]. The damping time scale $\tau_{\dot\theta}$=17.5 $\pm$ 0.5 s and the diffusivity $D_{\dot\theta} = (2.37 \pm 0.07) \times 10^{-6}$ rad^2/s^3 are fitted independently to the mean-square change in $\dot\theta_0$ over time as in [1]. The circulation rate ω_ϕ=0.022 $\pm$ 0.003 s^{-1} is obtained by first calculating the speed of the LSC as the distance $H/4$ between 2 vertically separated thermistors in the path of the LSC, divided by the time of peak correlation between their signals (16.6 $\pm$ 0.7 s), and further divided by the path length of the LSC, which is assumed to be between a rectangular path along a diagonal of length $2(1+\sqrt{2})H$ and a nearly ellipsoidal path of length $\pi(1+\sqrt{2})H/2$. With these parameter values and Eq. 3, the predicted switching rate $\omega = (0.9 \pm 0.6) \times 10^{-4}$ s^{-1}. This prediction is smaller than the measured switching rate $\bar\omega = 1.3 \times 10^{-4}$ s^{-1} (251 events measured over 21.7 days) by 40%, while consistent within error.

Alternatively, we can predict the parameter value $\tau_{\dot\theta} = 26.9$ s from the Navier-Stokes equations [1]. This value is higher than the independently measured value by 54%, increasing the predicted ω by 460%. This example indicates that the prediction of ω is very sensitive to parameter values, due to the exponential term in Eq. 3. This sensitivity means that the agreement within 40% for ω implies much better accuracy of 9% for individual model parameters. For our variation of cell dimensions of 0.7 mm (0.35%), ΔV_g could change by 0.95%, causing the predicted ω to change by 3.5%. This confirms our cell is still uniform enough to compare to predictions for a cubic cell.

To provide a stricter test of the model, we extend the prediction of switching rate ω to be a function of
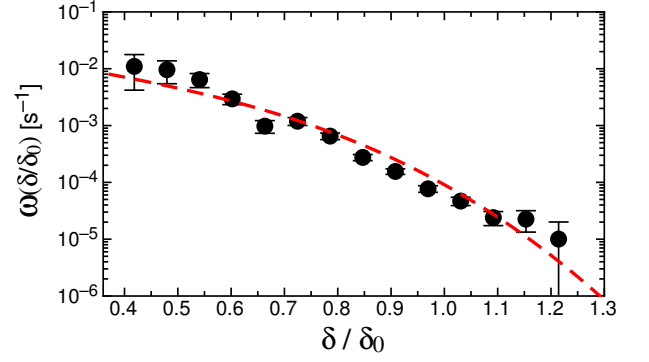

FIG. 6. The switching rate $\omega(\delta)$. Circles: measurements. Dashed line: model prediction from Eq. 4.

δ while still using the dynamics of δ from that original model. In principle, the fluctuations of δ around the stable fixed point δ_0 can affect both the damping and potential terms in Eq. 1. To account for this, we remove the model approximation of a fixed $\delta = \delta_0$ used in the original calculation of ω (Eq. 3) [1]. We can explicitly write the δ-dependence into the model since δ varies slowly, i.e. the timescale τ_δ that governs δ is much larger than the timescale $\tau_{\dot\theta}$ that governs θ_0 [1]. Thus, the damping timescale $\tau_{\dot\theta}$ in Eq. 3 can be replaced with $\tau_{\dot\theta}\delta_0/\delta$ as in Eq. 1. In addition, since ω_ϕ was assumed to be proportional to δ in the original model [1], but Eq. 2 was originally written with the implicit approximation $\delta = \delta_0$, ΔV_g can be generalized to $\Delta V_g(\delta) = \frac{3}{8}\left(1-\frac{\gamma}{2}\right)\left(\frac{\omega_\phi\delta}{\delta_0}\right)^2$. Using the same overdamped Kramers solution for the barrier crossing problem as in Eq. 3, the switching rate becomes

$$\omega(\delta) = \frac{\sqrt{c_{min}c_{max}}\tau_{\dot\theta}\delta_0}{2\pi\delta}\exp\left(-\frac{3\omega_\phi^2\delta^3}{8D_{\dot\theta}\tau_{\dot\theta}\delta_0^3}\left(1-\frac{\gamma}{2}\right)\right). \qquad (4)$$

This expression represents the rate of switching per unit time at each value of δ.

To compare this prediction with measurements, we calculate the corresponding measured value of $\omega(\delta)$ from $\omega(\delta) = \bar\omega P_s(\delta)/P(\delta)$, where $P(\delta)$ is the probability distribution of δ during an entire data set, and $P_s(\delta)$ is the distribution of δ during switching events. For each switching event, we use the value of δ the last time that θ_0 crosses the potential maximum.

Figure 6 shows a comparison of the measured δ-dependent switching rate $\omega(\delta)$ and the model prediction from Eq. 4. The trend of the data is captured well by the model, as the root-mean-square difference between measured and predicted $\omega(\delta)$ is 50% over 3 decades of ω. The δ-dependence in $\omega(\delta)$ leads to a modified prediction of the average switching rate: $\int \omega(\delta)P(\delta)d\delta = (1.7\pm1.1)\times10^{-4}$ s^{-1}, which is consistent with, and within 30% of the measured switching rate $\bar\omega = 1.3 \times 10^{-4}$ s^{-1}. However, this level of accuracy in $\bar\omega$ is better than we should expect,

since predictions of this model are typically only accurate within a factor of 2 or 3 due to the approximations made to obtain Eq. 1 [1], unless model parameters are fitted to data in non-independent measurements [36]. Regardless, the agreement between the predicted and measured $\omega(\delta)$ is exceptionally good for a low-dimensional model, considering parameter values $\tau_{\dot{\theta}}$, $D_{\dot{\theta}}$, and ω_ϕ are determined from independent measurements and the geometry dependence has no adjustable parameters.

The increase of the switching rate ω as δ decreases can be understood in terms of Eqs. 1 and 4. Small δ means a weaker LSC which leads to both smaller damping in Eq. 1 and potential barriers in Eq. 4. Both of these effects allow fluctuations to drive the system over the potential barriers more easily, resulting in a higher ω.

One notable advantage of this low dimensional model is its ability to get useful information about long-term dynamics from simulations. The parameters $\tau_{\dot{\theta}}$, $D_{\dot{\theta}}$, ω_ϕ, can be fitted by data from short-term simulations of only a few turnover times [1]. Once these parameters are obtained from short-term measurements, one could predict with high accuracy the statistics of rare events that occur once in ~ 100 turnover times, such as stochastic switching from Eq. 3 or cessations [5], without performing long-term simulations.

III. CONCLUSIONS

To summarize, we observe that LSC orientation θ_0 switches between corners by crossing potential barriers in θ_0 as a Poisson process, as predicted [1]. The prediction of the average switching rate $\bar{\omega}$ is 30% above the measured value, within error, while the prediction of $\omega(\delta)$ captures the trend in δ with a root-mean-square difference of only 50% over three decades of ω (Fig. 6). The switching can be understood as a turbulent-fluctuation-driven crossing of a potential barrier, where the potential is predicted from the shape of the sidewall. The switching is more likely to happen when δ is smaller, due to the decrease in both the potential barrier and damping.

In the bigger picture, the success of the prediction demonstrates that a low-dimensional turbulence model can quantitatively predict the existence and properties of a dynamical mode that did not exist in other geometries studied, without any flexibility or free parameters in the geometry-dependence of the model. The geometry-dependence of the model could be predicted without adjustable parameters because the low-dimensional model is derived from the Navier-Stokes equations. The key insight that allowed this derivation was that the robustness of the LSC allows it to be plugged in as an approximate solution. The remaining barrier to making predictions of the full model without any adjustable parameters is to predict the diffusivities that represent turbulent fluctuations – it remains an open question as to whether a general form for the stochastic term can be predicted based on turbulence statistics. This methodology can in principle be applied to other flows dominated by large-scale coherent structures. In other systems, the geometry-dependent term would have a different functional form, which we have shown can be predicted explicitly, and additional forcing terms would be different, so the dynamical equations and corresponding solutions would also be different, but the approach is one that potentially could lead to general, low dimensional turbulence models.

[1] E. Brown and G. Ahlers, Phys. Fluids **20**, 075101 (2008).
[2] E. Brown and G. Ahlers, Phys. Fluids **20**, 105105 (2008).
[3] R. Trapp, *Mesoscale-Convection Processes in the Atmosphere* (Cambridge Press, 2013).
[4] E. N. Lorenz, J. Atmos. Sci. **20**, 130 (1963).
[5] E. Brown and G. Ahlers, Phys. Rev. Lett. **98** (2007).
[6] A. de la Torre and J. Burguete, Phys. Rev. Lett. **99**, 054101 (2007).
[7] S. Thual, A. J. Majda, and S. N. Stechmann, Journal of the Atmospheric Sciences **71**, 697 (2014).
[8] G. Rigas, A. S. Morgans, , R. Brackston, and J. F. Morrison, J. Fluid Mech. (in review).
[9] P. Holmes, J. L. Lumley, and G. Berkooz, *Turbulence, Coherent Structures, Dynamical Systems, and Symmetry* (1996).
[10] G. Ahlers, S. Grossmann, and D. Lohse, Rev. Mod. Phys. **81**, 503 (2009).
[11] D. Lohse and K.-Q. Xia, Annu. Rev. Fluid Mech. **42**, 335 (2010).
[12] R. Krishnamurti and L. Howard, Proc. Natl. Acad. Sci. U.S.A. **78** (1981).
[13] S. Ciliberto, S. Cioni, and C. Laroche, Phys. Rev. E **54**, R5901 (1996).
[14] E. Brown and G. Ahlers, J. Fluid Mech. **568**, 351 (2006).
[15] H.-D. Xi, Q. Zhou, and K.-Q. Xia, Phys. Rev. E **73**, 056312 (2006).
[16] H.-D. Xi and K.-Q. Xia, Phys. Rev. E **75**, 066307 (2007).
[17] D. Funfschilling and G. Ahlers, Phys. Rev. Lett. **92**, 194502 (2004).
[18] E. Brown and G. Ahlers, J. Fluid Mech. **638**, 383 (2009).
[19] H.-D. Xi, S.-Q. Zhou, Q. Zhou, T.-S. Chan, and K.-Q. Xia, Phys. Rev. Lett. **102**, 044503 (2009).
[20] H. Song, E. Brown, R. Hawkins, and P. Tong, J. Fluid Mech. **740**, 136 (2014).
[21] K. R. Sreenivasan, A. Bershadskii, and J. J. Niemela, Phys. Rev. E **65**, 056306 (2002).
[22] R. Benzi, Phys. Rev. Lett. **95**, 024502 (2005).
[23] F. F. Araujo, S. Grossmann, and D. Lohse, Phys. Rev.

Lett. **95**, 084502 (2005).

[24] C. Resagk, R. d. Puits, A. Thess, F. V. Dolzhansky, S. Grossmann, F. F. Araujo, and D. Lohse, Phys. Fluids **18**, 095105 (2006).

[25] E. Brown and G. Ahlers, Phys. Fluids **18**, 125108 (2006).

[26] J.-Q. Zhong, S. Sterl, and H.-M. Li, J. Fluid Mech. **778** (2015).

[27] Y. Liu and R. E. Ecke, Phys. Rev. E **80**, 036314 (2009).

[28] E. Brown, A. Nikolaenko, D. Funfschilling, and G. Ahlers, Phys. Fluids **17**, 075108 (2005).

[29] G. Zocchi, E. Moses, and A. Libchaber, Physica A **166**, 387 (1990).

[30] X.-L. Qiu and K.-Q. Xia, Phys. Rev. E **58**, 486 (1998).

[31] Z. A. Daya and R. E. Ecke, Phys. Rev. Lett. **87**, 184501 (2001).

[32] T. Haramina and A. Tilgner, Phys. Rev. E **69**, 056306 (2004).

[33] S.-Q. Zhou, C. Sun, and K.-Q. Xia, Phys. Rev. E **76**, 036301 (2007).

[34] E. Brown, A. Nikolaenko, and G. Ahlers, Phys. Rev. Lett. **95**, 084503 (2005).

[35] H. A. Kramers, Physica **7**, 284 (1940).

[36] M. Assaf, L. Angheluta, and N. Goldenfeld, Phys. Rev. Lett. **107**, 044502 (2011).